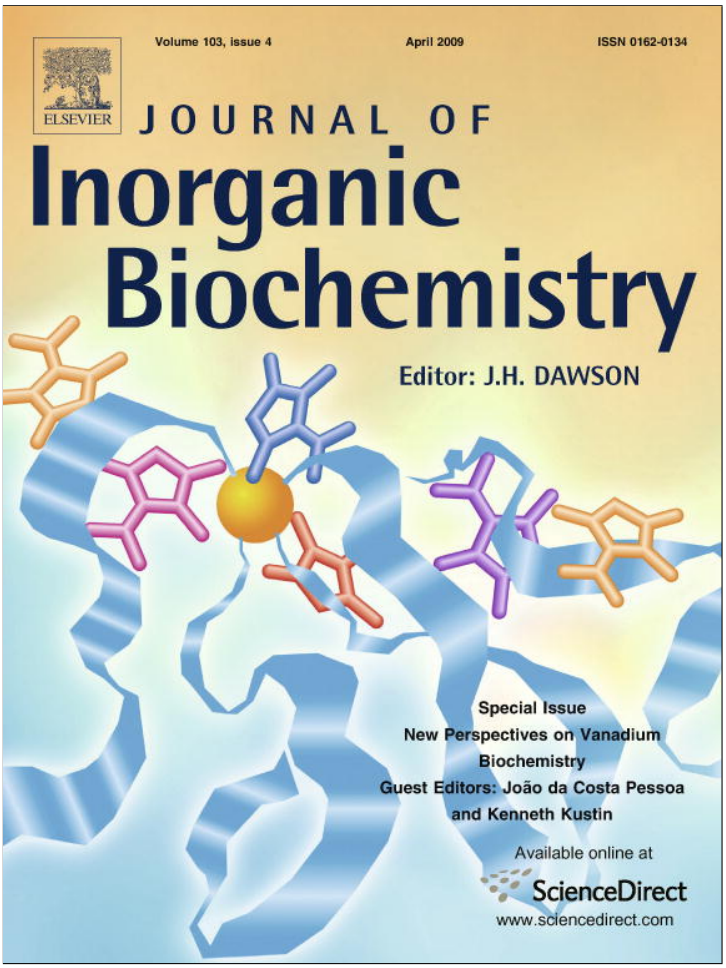

Journal of Inorganic Biochemistry 103 (2009) 487–495

Contents lists available at ScienceDirect

Journal of Inorganic Biochemistry

journal homepage: www.elsevier.com/locate/jinorgbio

Aminocarboxylate complexes of vanadium(III): Electronic structure investigation by high-frequency and -field electron paramagnetic resonance spectroscopy

Joshua Telser [a], Chi-Chin Wu [b], Kun-Yuan Chen [b], Hua-Fen Hsu [b,*], Dmitry Smirnov [c], Andrew Ozarowski [c], J. Krzystek [c,*]

[a] Department of Biological, Chemical and Physical Sciences, Roosevelt University, Chicago, IL 60605, USA
[b] Department of Chemistry, National Cheng Kung University, Tainan 701, Taiwan
[c] National High Magnetic Field Laboratory, Florida State University, 1800 E. Dirac Dr., Tallahassee, FL 32310, USA

ARTICLE INFO

Article history:
Received 25 August 2008
Received in revised form 5 January 2009
Accepted 7 January 2009
Available online 29 January 2009

ABSTRACT

Aminocarboxylate complexes of vanadium(III) are of interest as models for biologically and medicinally relevant forms of this interesting and somewhat neglected ion. The V(III) ion is paramagnetic, but not readily suited to conventional EPR, due to its integer-spin ground state ($S = 1$) and associated large zero-field splitting (zfs). High-frequency and -field EPR (HFEPR), however, has the ability to study such systems effectively. Three complexes, all previously structurally characterized: $Na[V(trdta)] \cdot 3H_2O$, $Na[V(edta)(H_2O)] \cdot 3H_2O$, and $[V(nta)(H_2O)_3] \cdot 4H_2O$ (where trdta stands for trimethylenediamine-*N*,*N*,*N*′,*N*′-tetraacetate and nta stands for nitrilotriacetate) were studied by HFEPR. All the investigated complexes produced HFEPR responses both in the solid state, and in aqueous solution, but those of $[V(nta)(H_2O)_3] \cdot 4H_2O$ were poorly interpretable. Analysis of multi-frequency HFEPR spectra yielded a set of spin Hamiltonian parameters (including axial and rhombic zfs parameters: D and E, respectively) for these first two complexes as solids: $Na[V(trdta)] \cdot 3H_2O$: $D = 5.60\ cm^{-1}$, $E = 0.85\ cm^{-1}$, $g = 1.95$; $Na[V(edta)(H_2O)] \cdot 3H_2O$: $D = 1.4\ cm^{-1}$, $E = 0.14\ cm^{-1}$, $g = 1.97$. Spectra in frozen solution yielded similar parameters and showed multiple species in the case of the trdta complex, which are the consequence of the flexibility of this ligand. The EPR spectra obtained in frozen aqueous solution are the first, to our knowledge, of V(III) in solution in general and show the applicability of HFEPR to these systems. In combination with very insightful previous studies of the electronic absorption of these complexes which provided ligand-field parameters, it has been possible to describe the electronic structure of V(III) in $[V(trdta)]^-$ and $[V(edta)(H_2O)]^-$; the quality of data for $[V(nta)(H_2O)_3]$ does not permit analysis. Qualitatively, six-coordinate V(III) complexes with O,N donor atoms show no electronic absorption band in the NIR region, and exhibit relatively large magnitude zfs ($D \geqslant 5\ cm^{-1}$), while analogous seven-coordinate complexes do have a NIR absorption band and show relatively small magnitude zfs ($D < 2\ cm^{-1}$).

1. Introduction

Vanadium has long been an appealing transition metal for study due to its wide range of oxidation states and associated beautiful colors of its complexes [1]. Among these oxidation states, V(III) has traditionally been less studied than V(IV) or V(V), which have better defined biological/physiological roles [2]. Interest in V(III) has recently increased due to the observation of V(III) in marine organisms, namely in the blood cells of sea squirts (subphylum Tunicata; class Ascidiacea) [3–5]. The specific observation of V(III) was first shown by Taylor et al. [6] although the original observation of vanadium in tunicates dates back to nearly a century ago [7], before there was such an area as bioinorganic chemistry. Another biological aspect of V(III) is that its complexes have been promoted as insulin mimics/anti-diabetic agents [8,9], although are less effective than V(IV) and V(V) in this role [10,11].

Duplication of the exact ligands found in tunicates is challenging; however, such a coordination environment can be modeled by the use of aminocarboxylate ligands. These widely used ligands support V(III) in stable complexes that are also models for the insulin-mimetic species. We therefore have performed an initial study on aminocarboxylate complexes of V(III), primarily employing HFEPR with the goal of furthering our understanding of the electronic structure of these systems, in both six- and seven-coordinate geometries.

In contrast to V(IV), with its $3d^1$ electronic configuration and $S = 1/2$ spin ground state, which can be fruitfully studied by conventional (e.g., X-band, ~9 GHz) EPR [12], V(III), $3d^2$, $S = 1$ has been much less easily studied by EPR. An integer-spin (non-Kramers) ion

* Corresponding authors. Tel.: +886 6 2757575x65336; fax: +886 6 2740552 (H.-F. Hsu), tel.: +1 850 644 6077; fax: +1 850 644 1366 (J. Krzystek).
E-mail addresses: konopka@mail.ncku.edu.tw (H.-F. Hsu), krzystek@magnet.fsu.edu (J. Krzystek).

0162-0134/$ - see front matter © 2009 Elsevier Inc. All rights reserved.
doi:10.1016/j.jinorgbio.2009.01.016

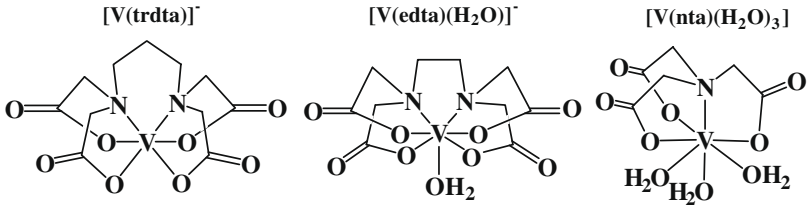

Scheme 1.

such as V(III) is susceptible to zero-field splitting (zfs). In axial symmetry, the $\langle S, M_S| = \langle 1,0|$ and $\langle 1,\pm1|$ states are separated by an energy gap equal to the parameter D. If D is sufficiently large in magnitude, then this gap is too large for the ($\Delta M_S = \pm1$) transitions between the $\langle 1,0|$ and $\langle 1,\pm1|$ states to appear at X-band frequencies, where the microwave quantum is $\sim$0.3 cm^{-1} and the given complex is deemed 'EPR-silent'. This difficulty of observing EPR can be overcome by the use of high frequencies going into sub-THz and THz range (on the order of 100 cm^{-1}) with correspondingly high resonant magnetic fields (up to 45 T in a continuous mode at the NHMFL in Tallahassee; higher fields operated in a pulsed mode are used at the NHMFL operation in Los Alamos, and elsewhere [13]). This technique is referred to as HFEPR and has been successfully applied to a wide variety of non-Kramers systems [14,15], including V(III) [16–21]. All of these systems were studied in the solid state, usually as a pure powder, although in some cases as a doped single crystal [17,19]. HFEPR spectra in frozen solution have been reported for non-Kramers ions such as Cr(II) [22] and Mn(III) [23], but not for V(III). One limitation is the relatively high solubility necessary for HFEPR in frozen solution (in our experience, concentrations at least 100 mM are ideal for V(III) and other non-Kramers systems, with $\sim$10 mM an absolute minimum); however, $[V(H_2O)_6]^{3+}$ can be generated in very high concentration in aqueous solution, yet we have been unable to reproducibly observe the expected HFEPR signals from this complex. Aminocarboxylate complexes also exhibit very high solubility and are thus good candidates for observation of HFEPR in frozen aqueous solution. The specific complexes investigated are those of V(III) with trdta, edta, and nta. Their structures are shown in cartoon form in Scheme 1, and are representative of six- and seven-coordinate aminocarboxylate complexes of V(III). The actual coordination geometry of these complexes, based on X-ray crystallography, can be seen in Fig. S1 (Supplementary material). In all of these complexes it was possible to observe HFEPR responses in frozen aqueous solution, which, to our knowledge is the first such result for a complex of V(III).

The spin Hamiltonian parameters provided by analysis of the HFEPR spectra of these systems can be combined with analysis of their electronic absorption spectra [24] to yield a characterization of the ligand field experienced by V(III) with aminocarboxylate ligands. This information could then be applied to V(III) in biological or physiological environments, such as in ascidians or insulin-mimetic cases.

2. Experimental

2.1. Materials

All starting materials were obtained commercially and used without further purification. The complexes $Na[V(trdta)] \cdot 3H_2O$[1] [25], $Na[V(edta)(H_2O)] \cdot 3H_2O$ [26], and $[V(nta)(H_2O)_3] \cdot 4H_2O$ [27] were prepared following literature procedures and characterized by elemental analysis: For $Na[V(trdta)] \cdot 3H_2O$ ($C_{11}H_{20}N_2NaO_{11}V$): calculated C, 30.71%; H, 4.69%; N, 6.51%; found C, 30.43%; H, 4.72%; N, 6.49%. For $Na[V(edta)(H_2O)] \cdot 3H_2O$ ($C_{10}H_{20}N_2NaO_{12}V$): calculated C, 27.66%; H, 4.64%; N, 6.45%; found C, 27.04%; H, 4.80%; N, 6.29%. For $[V(nta)(H_2O)_3]$ ($C_6H_{12}NO_9V$): calculated C, 24.59%; H, 4.13%; N, 4.78%; found C, 25.63%; H, 4.36%; N, 5.01%. The appearance of these complexes is sensitive both to degree of hydration and to crystal morphology. In our hands, $Na[V(trdta)] \cdot 3H_2O$ displays a pale pinkish color when crystallized from H_2O/ethanol or H_2O/THF; however, after washing and drying *in vacuo*, the compound exhibits a reddish color. A reddish color for $Na[V(trdta)] \cdot 3H_2O$ has also been reported by Robles et al. [25]. $Na[V(edta)(H_2O)] \cdot 3H_2O$ appears as the greyish green material described by Shimoi et al. [26], who reported the crystal structure. The original synthesis of this complex, by Schwartzenbach and Sandera [28], described grey crystals as well.

2.2. Electronic absorption spectroscopy

Electronic absorption spectra were recorded on aqueous solutions of $[V(trdta)]^-$ and $[V(edta)(H_2O)]^-$ over the range 300–1100 nm, using a Hewlett Packard 8453 spectrophotometer. The spectra of both complexes were in agreement with those found in the literature [24,29].

2.3. HFEPR spectroscopy

HFEPR spectra were recorded using the Millimeter and Sub-millimeter Wave Facility at NHMFL [30], and the EMR Facility. The former experimental setup employs tunable frequencies in the 70 GHz–1.2 THz range (of which the 150–700 GHz range was used in this study) and the resistive "Keck" magnet enabling 0–25 T field sweeps, while the latter utilizes a variety of solid state sources and a superconducting 15 T magnet. Detection was provided with an InSb hot-electron bolometer (QMC Ltd., Cardiff, UK). Modulation for detection purposes was provided alternatively by chopping the sub-THz wave beam ("optical modulation") or by modulating the magnetic field. A Stanford Research Systems SR830 lock-in amplifier converted the modulated signal to DC voltage.

Typically, 30–50 mg of polycrystalline sample was used for HFEPR on solid samples. In previous HFEPR studies of magnetically non-diluted paramagnetic solids, magnetic field-induced torquing of microcrystallites occurred [31]. In this work, such effects were generally not observed.

For solution studies of V(III) aminocarboxylates, two methods were used. In the first case, the solid was dissolved in degassed, deionized water, without adjustment of pH, and then rapidly frozen before placement into the sample holder. This method was suitable for use with $Na[V(edta)(H_2O)] \cdot 3H_2O$, as it has been shown that $[V(edta)(H_2O)]^-$ in solution maintains the same species from pH 1.8 to 7.5 [29]. However, for $Na[V(trdta)] \cdot 3H_2O$ and $[V(nta)(H_2O)_3] \cdot 4H_2O$, we found that this method led to incomplete dissolution of solid (this problem was not readily apparent due to the

[1] The abbreviation tmdta is also commonly used; this ligand is also referred to as 1,3-diaminopropane-*N*,*N*,*N*′,*N*′-tetraacetate, so the abbreviation pdta is also encountered.

dark color of highly concentrated solutions, the small volumes involved, and the need to avoid air exposure) [25]. Therefore, a second method was used in which the solid was placed under nitrogen into degassed water that had been adjusted to pH < 2 by addition of sulfuric acid. The pH was then raised by addition of NaOH during which time the solid could be seen to dissolve with formation of the characteristic dark red color of aqueous $[V(trdta)]^-$. This procedure was also used to prepare solutions of $[V(nta)(H_2O)_3]$. Solution concentrations were approximately 200 mM.

2.4. X-band EPR spectroscopy

X-band EPR experiments were performed on a commercial Bruker ElexSys E680X spectrometer equipped with a low-temperature Oxford Instruments ESR900 cryostat.

2.5. EPR analysis

The magnetic properties of an ion with $S = 1$ can be described by the standard spin Hamiltonian comprised of Zeeman and zfs terms [32]:

$$\mathscr{H} = \beta B \cdot \mathbf{g} \cdot S + D(S_z^2 - S(S+1)/3) + E(S_x^2 - S_y^2). \quad (1)$$

Field-swept HFEPR on polycrystalline solids or low-temperature glasses provides turning points in powder-pattern spectra. Their frequency dependencies were recorded as two-dimensional data sets, and spin Hamiltonian parameters were then fitted to these data by use of a non-linear least-squares procedure based on the well-known formulas resulting from the exact solution of the equations for triplet states of arbitrary orientation [33]. Further details of the tunable-frequency EPR methodology are given elsewhere [14]. In other cases, notably those of relatively small magnitude of zfs, we obtained the spin Hamiltonian parameters by simulating single-frequency spectra.

2.6. AOM analysis

Analysis of the electronic structure of V(III) in aminocarboxylate complexes was performed with use of the angular overlap model (AOM) [34]. Two computer programs were employed, Ligfield, written by Bendix et al. (Ørsted Institute, Copenhagen, Denmark) [35] and a locally-written program, DDN, which is available from J. Telser. Both programs use the complete d^2 weak-field basis set including inter-electronic repulsion (Racah parameters: B, C) [34,36], spin-orbit coupling (SOC constant: ζ) [35], and AOM ligand-field bonding parameters (ε_σ and ε_π) [37], and gave identical results when directly compared. The Racah parameters for free-ion V(III) are variously given as follows: $B = 886\ cm^{-1}$, $C = 4.7B$ [34]; or $B = 860\ cm^{-1}$, $C = 4.8B$ [36]; while $C = 5B$ was used by Schönherr et al. for V(III) in these specific systems [38]. We explored the effect of values in the range $4.5 \leqslant C/B \leqslant 5.0$. Values for the SOC constant are available in a number of sources; however, the definitive value is that determined by Bendix et al.: $\zeta = 206\ cm^{-1}$ [35].

DDN allows use of a non-linear least-squares fitting subroutine (DSTEPIT, from QCPE, Bloomington, IN) to match observed electronic transition energies to those calculated by user-defined variable parameters such as B, ε_σ, etc. The general AOM procedure involved an initial fit of spin-allowed optical transitions with variation of Racah B and AOM bonding parameters, and with $\zeta \equiv 0$. From this initial fit, ζ was systematically varied until a reasonable match obtained for $|D|$ in relation to experimental values. The resulting electronic transitions were then checked to ensure that they were still in agreement with experiment; if not, then the AOM parameters were adjusted to correct discrepancies. DDN also allows inclusion of an external magnetic field to be applied along the molecular axes (defined by the AOM) to give Zeeman splitting of energy levels from which g values can be calculated, as described previously [16].

3. Results and discussion

3.1. X-ray crystallography

A search of the Cambridge Structural Database (CSD 5.29, November 2007 release) reveals a number of structures of aminocarboxylate complexes of V(III). Of specific relevance here are the structures of $Na[V(trdta)] \cdot 3H_2O$ (CSD code: PATZIT [25]), $Na[V(edta)(H_2O)] \cdot 3H_2O$ (CSD code: VEFKOG10 [26]; these workers also reported structures of edta complexes of V(III) with other counter cations), $[V(Hedta)(H_2O)] \cdot H_2O$ (CSD code: YUCMEO [39]), and $[V(nta)(H_2O)_3] \cdot 4H_2O$ (CSD code: VOXCUG [27]). The molecular structures of $Na[V(trdta)] \cdot 3H_2O$, $Na[V(edta)(H_2O)] \cdot 3H_2O$, and $[V(nta)(H_2O)_3] \cdot 4H_2O$ are shown together in Fig. S1 (Supplementary material). Also shown are packing diagrams for each complex, respectively, in Figs. S2, S3, and S4. The H-bonding network in each of these complexes is different.

Most of these V(III) complexes (as well as other related complexes not studied here [40,41]) exhibit interesting seven-coordinate geometries. A discussion of some of the complexities of seven-coordinate geometries is given by Dreyer et al. [42]. $[V(edta)(H_2O)]^-$ adopts a capped trigonal prismatic geometry, which can also be described as 4:3 piano stool (tetragonal base-trigonal base) [26]. $[V(Hedta)(H_2O)]$ also has a structure close to a mono-capped trigonal prism [39], and $[V(nta)(H_2O)_3]$ exhibits a structure that can be described as a mono-capped octahedron, rather than a trigonal prism [27]. In contrast, $[V(trdta)]^-$ is a distorted octahedral complex, with only the sexidentate trdta ligand and without a coordinated aqua/hydroxo ligand [25]. Robles et al. were the first to suggest that in contrast to the five-membered rings formed with nta or ethylenediamine-based ligands, trdta forms a six-membered ring with V(III) and is unlikely to form seven-coordinate complexes[25]. This was explained further by Meier et al. in terms of the geometric requirements of seven- vs. six-coordination with the former requiring a bite angle that would severely strain a six-membered chelate ring [24]. However, in previous studies of V(III) complexes with a tripodal PS3 ligand and its derivatives (PS3 = trisbenzenethiolatophosphine) by some of us, it was found that the geometries of V(III) complexes are very flexible with little relevance of the size of the chelate ring [43]. Furthermore, the crystal structure of a seven-coordinate complex of sexidentate trdta with Mn(II), $[Mn(trdta)(H_2O)]^{2-}$, has been recently reported [44]. It is thus quite possible that seven-coordinate V(III) complexes of trdta form in solution as well.

3.2. Electronic absorption spectroscopy

Electronic absorption spectroscopic studies of aminocarboxylate complexes of V(III) have been previously reported in detail by Meier et al. for both $Na[V(trdta)] \cdot 3H_2O$ and $Na[V(edta)(H_2O)] \cdot 3H_2O$ [24] and also by Kanamori et al. for $Na[V(trdta)] \cdot 3H_2O$ [29]. These workers have all pointed out that diffuse reflectance spectra in the solid state for these complexes are essentially the same as in solution. We have reproduced their aqueous solution electronic absorption spectra as shown in Figs. S5 and S6.

$[V(trdta)]^-$ exhibits three well defined bands at $27{,}500\ cm^{-1}$, $22{,}900\ cm^{-1}$, and $18{,}100\ cm^{-1}$, but no significant absorption in the NIR region. There is a question as to exactly what solution species give rise to this spectrum. Two major species are likely present while dissolving $Na[V(trdta)] \cdot 3H_2O$ in aqueous solution (the solution might not be neutral): a six-coordinate complex, $[V(trdta)]^-$,

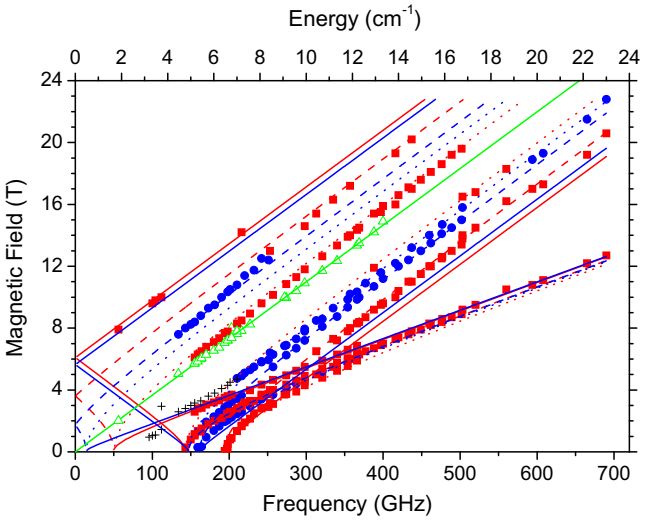

Fig. 1. Field vs. frequency map of EPR resonances recorded at 5 K for solid Na[V(trdta)] · $3H_2O$. Red squares represent experimental resonances attributed to the dominant triplet state of somewhat larger zfs parameters than that represented by the blue circles. Red curves were simulated using $S = 1$, $|D| = 5.60\ cm^{-1}$, $|E| = 0.85\ cm^{-1}$, $g_{iso} = 1.95$, and blue curves using $S = 1$, $|D| = 5.15\ cm^{-1}$, $|E| = 0.23\ cm^{-1}$, $g_{iso} = 1.95$, with dotted lines represent turning points with $B_0||x$, dashed lines with $B_0||y$ and solid lines with $B_0||z$. Black crosses at low frequencies/fields represent resonances that could not be attributed to either triplet state; their appearance suggests a presence of yet another species characterized by a smaller zfs. Green triangles are resonances originating from a V(IV) impurity as proved by the green line, which is a simulation using $S = 1/2$ and $g_{iso} = 1.95$.

in which all of the donor atoms of the ligand are coordinated, which presumably corresponds to the crystal structure [25], and another six-coordinate complex, $[V(trdta)(H_2O)]^-$ in which one pendant carboxylate arm is not coordinated with a water ligand taking up this site [29]. In addition to the equilibrium in solution between these two species, and conformational effects of the propane linker group (see below), the hydroxo complex, $[V(trdta)(OH)]^{2-}$ and the dinuclear oxo-bridged complex, $[V_2(trdta)_2(\mu\text{-}O)]^{4-}$ can form at higher pH values. In our studies, we have controlled the solution pH so that these high-pH species should not be present.

$[V(edta)(H_2O)]^-$exhibits a major band at 22,400 cm^{-1}, with shoulders at ~25,400 cm^{-1} and ~28,000 cm^{-1}, and a partially resolved band at 19,600 cm^{-1}. There is also a band at 12,500 cm^{-1}, and a broad band in the NIR extending from ~9500 cm^{-1} beyond the spectrometer range.

Kanamori et al. [29] have also employed a variety of other techniques to study aminocarboxylate complexes of V(III), such as spin-lattice relaxation time by ^1H NMR, and resonance Raman spectroscopy as well as UV–Vis as a function of pH, all of which demonstrated that $[V(edta)(H_2O)]^-$ in solution maintains the same species from pH 1.8 to 7.5. An equilibrium between $[V(edta)(H_2O)]^-$ and $[V(edta)(OH)]^-$ is present in solution above pH 7.5; however, in our solution HFEPR studies the pH was always kept below this value. We can be confident, therefore, that all HFEPR studies of the edta complex are of $[V(edta)(H_2O)]^-$.

3.3. HFEPR spectroscopy

The three complexes were each investigated in the solid state over a wide range of frequencies and temperatures. Each complex will be described separately.

3.3.1. Na[V(trdta)] · $3H_2O$

This complex exhibited strong resonances from V(III) over a very wide field range at typical frequencies, corresponding to a multitude of zero-field splitting parameters, some reaching quite large values ($D > 5\ cm^{-1}$). Experiments on a solid state sample allowed us to detect and characterize the triplet state with the largest zfs parameters by tunable-frequency methodology. Fig. 1 shows the field vs. frequency map as detected experimentally together with the simulated curves. Another triplet species, with somewhat smaller zfs, and of apparently lower concentration, has also been identified in the field/frequency map, but its parameters cannot be determined as accurately as those for the dominant species. Spin Hamiltonian parameters used in simulations for these two components are summarized in Table 1. The magnitude of D determined for the dominant species in solid Na[V(trdta)] · $3H_2O$, 5.60 cm^{-1}, is similar to that for $[V(H_2O)_6]^{3+}$, as found in a variety of V(III)-doped group 13 alums, of general formula $Cs[M(H_2O)_6](SO_4)_2$ (M = Al, Ga, In), for which very high precision spin Hamiltonian parameters were extracted from a high-quality single-crystal HFEPR study by Tregenna-Piggott et al. [19]. For example, V(III)-doped $Cs[Ga(H_2O)_6](SO_4)_2$ had $D = +4.8581\ cm^{-1}$ (these high symmetry (S_6 point group) systems have perfectly axial zfs ($E = 0$); the positive sign of D is surmised from their Fig. 6). Likewise, $V(acac)_3$, another complex with an O6 donor set, studied by some of us earlier [16], gave $D = +7.470\ cm^{-1}$, $E = +1.916\ cm^{-1}$ (E is given the same sign as D by convention). We were not able to determine the sign of D in solid Na[V(trdta)] · $3H_2O$; however, we assume that it is positive as in these other V(III) complexes. There is also an indication of yet other, minor triplet states observed in solid complex, characterized by much smaller magnitudes of D than the major species.

Table 1
Spin Hamiltonian parameters for aminocarboxylate complexes of V(III).

Complex	D (cm^{-1})[a]	E (cm^{-1})[a]	g[b]
Na[V(trdta)] · $3H_2O$ (solid)	5.60[c]	0.85	1.95
$[V(trdta)]^-$ (aqueous solution)	+0.87[d]	0	$g_{x,y} = 1.98$, $g_z = 1.95$
	+0.62	0	$g_{x,y} = 1.98$, $g_z = 1.95$
Na[V(edta)(H_2O)] · $3H_2O$ (solid)	1.4	0.14	1.97
$[V(edta)(H_2O)]^-$(aqueous solution)	+2.01	0.0	1.95
[V(nta)(H_2O)$_3$] · $4H_2O$(solid)	Not determined[e]	Not determined	1.96
[V(nta)(H_2O)$_3$](aqueous solution)	+0.6	+0.1	1.96

[a] The sign of D is given where determined while the sign of E is assumed to be same as that of D.
[b] The g value determination is isotropic, except where indicated.
[c] Another triplet state with somewhat smaller zfs and of lower concentration has been also identified from the field/frequency map with $|D| \cong 5.15\ cm^{-1}$, $|E| \cong 0.23\ cm^{-1}$, $g_{iso} \cong 1.95$.
[d] In addition to the two triplet species listed here, another triplet state with larger zfs has been also identified in the spectra with $|D| \cong 2.35\ cm^{-1}$, $|E| \cong 0$, $g_{iso} \cong 1.95$.
[e] Strong spin exchange in solid [V(nta)(H_2O)$_3$] · $4H_2O$ averages the zfs.

An HFEPR study of $[V(trda)]^-$ in *frozen aqueous solution* allowed us to detect and characterize some of those states. Fig. 2 shows a solution spectrum recorded at 305 GHz, and 20 K. Even a perfunctory analysis of this spectrum shows that multiple triplet states are contributing to it. We have attempted to deconvolute this spectrum and have extracted three distinct triplet species. Two of these are very similar; one being described by $D = 0.68\ cm^{-1}$ and another with 0.87 cm^{-1}. In neither case could the rhombic parameter E be resolved. The third triplet species identified has a much larger D value (~2.35 cm^{-1}) and is also characterized by a much larger linewidth. Fig. 2 therefore displays a simulated spectrum that is the sum of the three triplet species identified, in equal amounts. The individual simulations for these three triplet species are shown

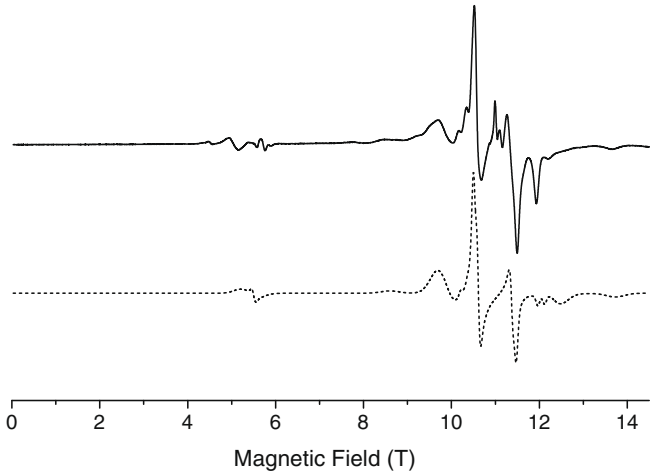

Fig. 2. HFEPR spectrum of aqueous $[V(trdta)]^-$ recorded at 305 GHz and 20 K (solid trace) together with a simulation (dashed trace) assuming an ideal powder pattern, which is the sum of equal amounts of three individual triplet species. Spin Hamiltonian parameters used in the simulations: all $S = 1$; one species with: $D = +0.68$ cm^{-1}, $E = 0$, $g_{x,y} = 1.98$, $g_z = 1.95$, 50 mT isotropic single-crystal linewidth; one species with $D = +0.87$ cm^{-1}, $E = 0$, $g_{x,y} = 1.98$, $g_z = 1.95$, 50 mT linewidth; one species with: $D = +2.35$ cm^{-1}, $E = 0$, $g_{iso} = 1.95$, 200 mT linewidth. Simulations of the individual species are shown in Fig. S7 in the Supplementary material. The sharp peaks appearing near 11 T in the experiment are due to a V(IV) impurity and not reproduced in the simulation.

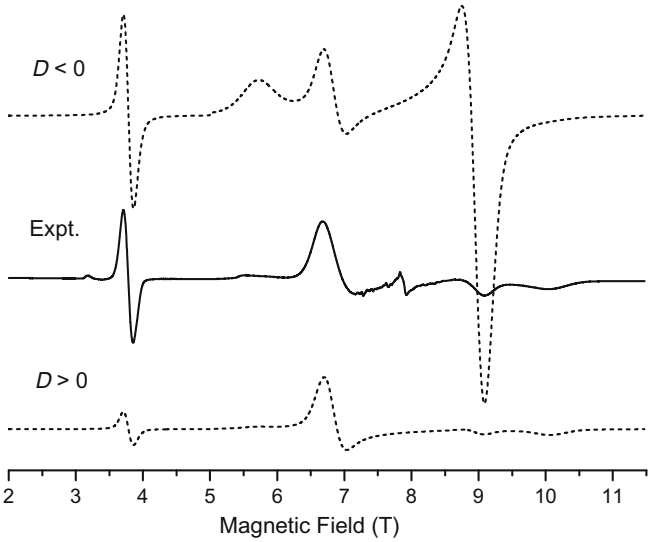

Fig. 3. HFEPR spectrum of aqueous $[V(edta)(H_2O)]^-$ recorded at 218 GHz and 20 K. Central (solid) trace: experiment; upper dashed trace: simulation using parameters: $S = 1$, $D = -2.01$ cm^{-1}; $E = 0$, $g_{iso} = 1.95$; lower dashed trace: simulation using the same value but a positive sign of D. Isotropic single-crystal linewidth used in the simulations for the $\Delta M_S = \pm 1$ transitions: 200 mT; for the $\Delta M_S = \pm 2$ transition: 50 mT. The intensities of the simulated spectra are scaled so as to match exactly the experimental turning point at 6.8 T, demonstrating that the intensities of the features at 5.9, 9 and 10 T are matched by the simulation only for $D > 0$. The peak near 8 T originates from a trace amount of V(IV) impurity and is not reproduced in the simulations, and neither is the weak resonance near 3.2 T, which is due to solid molecular dioxygen in the sample space.

in Fig. S7, and an analogous analysis at a lower frequency of 197 GHz, in Fig. S8.

3.3.2. $Na[V(edta)(H_2O)] \cdot 3H_2O$

Strong resonances attributable to V(III) were observed for the solid sample at a variety of field/frequency combinations. The quality of spectra (not shown) was, however, poor due to the impossibility of obtaining a satisfactory powder distribution of the crystallites, and the concomitant pseudo-noise in the spectra, as has been seen elsewhere [22]. The spin Hamiltonian parameters could thus only be estimated semi-quantitatively from such spectra as $|D| \sim 1.4$ cm^{-1}, $|E| \sim 0.14$ cm^{-1}, $g_{iso} = 1.97$.

Frozen aqueous solutions of $[V(edta)(H_2O)]^-$ produced, on the other hand, almost ideal powder-patterned EPR spectra, as shown in Fig. 3, again accompanied by simulations. Thus, the triplet state detected in frozen aqueous solution at 20 K is characterized by $|D|$ almost exactly equal to +2 cm^{-1} and an axial zfs tensor ($E \sim 0$). The positive sign of D was established by a comparison to simulations produced using both positive and negative values of that parameter, as shown in Fig. 3.

3.3.3. $[V(nta)(H_2O)_3] \cdot 4H_2O$

This sample investigated as a solid produced a single, symmetrical resonance at $g = 1.96$ at any frequency (Fig. S9). The origin of this line was difficult to ascertain until an aqueous solution experiment was performed (see below). In retrospective, it is due to a triplet state of V(III) averaged through an efficient spin exchange taking place in the crystal. The nature of this exchange is beyond the scope of this paper, but it is a qualitatively different situation than found in either of the two other complexes studied here as solids, or other V(III) complexes investigated by HFEPR previously [16]. In view of this phenomenon, the zfs parameters in the solid state could not be determined. Upon dissolution in water, the exchange between the individual complexes is cancelled, and a spectrum readily attributed to a triplet state observed (Fig. S9). However, this spectrum suffers from low resolution of its components, thus only a semi-quantitative set of spin Hamiltonian parameters was obtained through simulations: $D \sim 0.6$; $E \sim 0.1$ cm^{-1}, $g_{iso} = 1.96$.

3.4. X-band EPR spectroscopy

The high quality of spectra, and the moderate value of D in $[V(edta)(H_2O)]^-$ prompted us to perform a conventional (X-band) EPR study of the same complex in a frozen aqueous solution. Indeed, we were able to record distinct if broad resonances belonging to the V(III) spin manifold besides the ubiquitous, sharp signals originating from a V(IV) impurity. The 9.7 GHz EPR spectrum, which is shown in Fig. 4, can be fairly well simulated using the same set of zfs parameters as obtained from the HFEPR experiment; however, reversing the procedure, i.e., obtaining those parameters from a low-frequency experiment alone would be an almost impossible task. We note that the single-crystal linewidths needed for the X-band simulations are comparable in breadth to those used at high frequencies. This points at D-strain (i.e., distribution in D and E values; a field-independent phenomenon), as opposed to g-strain, which is field-dependent, as a major factor contributing to the linewidths in V(III) spectra. Detailed analyses of linewidths in HFEPR of high-spin systems have been performed in other cases [45], but are beyond the scope of this study.

3.5. Ligand-field analysis of V(III) complexes

The spin Hamiltonian parameters derived from HFEPR, in combination with the electronic absorption spectra, with the crystal structures, and with previous work [24,38], in principle allow a quantitative description of the electronic structure of V(III) in each of these complexes. In practice, the trdta and edta complexes provide the necessary data, while the nta complex does not. The lack of spin Hamiltonian parameters for solid $[V(nta)(H_2O)_3] \cdot 4H_2O$ means that we cannot relate a known structure to a known set of parameters. Spin Hamiltonian parameters were estimated for $[V(nta)(H_2O)_3]$ in solution, but analysis suffers from the same difficulties as $[V(trdta)]^-$ in terms of multiple solution species (see below), if not more so, since nta has a lower denticity than trdta (or

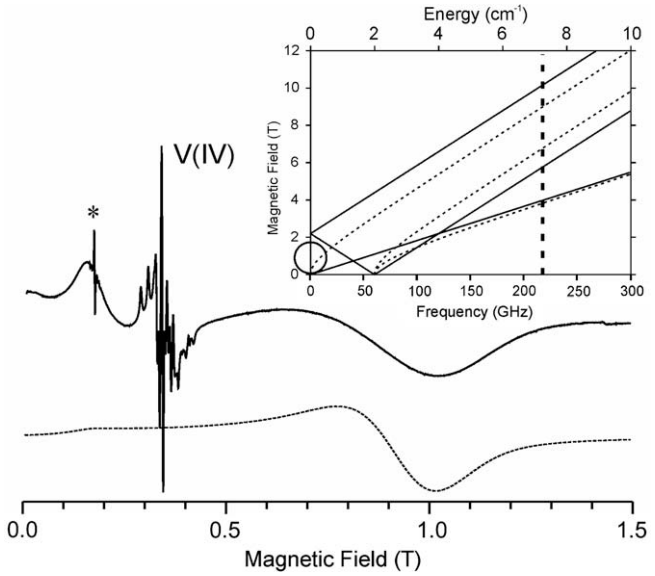

Fig. 4. Main figure: $[V(edta)(H_2O)]^-$ in aqueous solution shows spectra even at X-band (at 9.7 GHz and 20 K; upper, solid trace is experiment; lower, dashed trace is simulation using the spin Hamiltonian parameters obtained from HFEPR experiments, with the single-crystal linewidth of 100 mT for the perpendicular turning point, and 25 mT for the parallel one; these linewidths are of the same order of magnitude as those required at high frequencies). The group of resonances centered on 350 mT belongs to the well-known hyperfine pattern of the VO^{2+} ion. The single narrow line at ca. 180 mT, indicated by the asterisk, originates from the dielectric resonator used in this experiment. Inset: the origin of the 218 GHz, and 9.7 GHz resonances in the 2D field/frequency representation such as in Fig. 1 (solid lines are with the field parallel; dashed lines with the field perpendicular to the molecular axes). The field range of the HFEPR experiment (see Fig. 3) is represented by the vertical dotted line, while the circle indicates the X-band EPR conditions used here.

edta). For the nta complex, we therefore make only the qualitative conclusion that the low magnitude of D observed in frozen solution is consistent with a seven-coordinate complex, consistent with the crystal structure and with the results for the edta complex, and in contrast to six-coordinate $Na[V(trdta)] \cdot 3H_2O$ (see Table 1).

We now proceed to a quantitative analysis of the results for the trdta and edta complexes. Meier et al. have performed a detailed analysis of the electronic absorption spectra in aqueous solution at room temperature and in the solid state at low temperature of two of the complexes of V(III) studied here: $Na[V(trdta)] \cdot 3H_2O$ and $Na[V(edta)(H_2O)] \cdot 3H_2O$ [24]. Their analysis made use of the AOM, and a complete set of bonding parameters (e_σ and e_π) for the aqua O (for the edta complex), carboxylato O, amine N ligands were reported. They did not provide fit values for the Racah parameter B; however, a later paper did provide this value for each complex [38]. Meier et al. also did not tabulate any values for either experimental or calculated band positions; however, we surmise from their published figures that an excellent match between the two was obtained [24,38]. A further unfortunate complication is that these workers did not describe the geometrical models for using their parameters; however, this was later provided to us, in the case of $[V(edta)(H_2O)]^-$, by Prof. T. Schönherr (personal communication). We have therefore derived our own models for using the AOM in these complexes.

In the case of $Na[V(trdta)] \cdot 3H_2O$, we begin by making the assumption that the major component seen by HFEPR is associated with the structure characterized crystallographically. The presence of minor species in the polycrystalline material studied by HFEPR likely results from complexes with slight structural differences derived from different association/H-bonding of the waters of hydration and/or degrees of hydration. Previous experience has shown that spin Hamiltonian parameters, derived from HFEPR, are very sensitive to slight changes in coordination that are unidentifiable by other methods [46,47].

With this proviso, the choice of geometrical model for the six-coordinate trdta complex is relatively straightforward, despite the severe distortion from octahedral symmetry. A model was chosen in which the molecular z-axis is along the O3-V-O5 vector, since this is the unique, all oxygen donor, axis (the other two both being O(1,7)-V-N(2,1)). The O3-V-O5 bond angle is 166.85°, however we idealize it at 180°, and take averages of the angle from a given atom to the V-O3,5 vectors. The molecular x-axis was chosen as the bisector of the N1-V-N2 plane (see Fig. 5; the specific angular parameters are given in Table S1).

Use of this geometrical model and the entire set of parameters provided by Schönherr and co-workers [38] provides a good fit to the observed electronic transitions, making "fine-tuning" of their parameters superfluous. The calculated transition energies are given in Table S2. Their value for the Racah parameter $B = 580\ cm^{-1}$, is ~65–67% of the free-ion value [34,36], which is reasonable for a covalently bonded complex [34]. Inclusion of spin-orbit coupling, with $\zeta = 140\ cm^{-1}$, 68% of the definitive free-ion value – the same ratio as for B, gives zero-field splitting with the same sign and magnitude as that observed for the major component of solid $Na[V(trdta)] \cdot 3H_2O$ (see Table 2). The degree of rhombicity is somewhat overstated by the calculation ($|E/D| = 0.32$ calculated vs. 0.15 by experiment), but this is hardly a major deficiency, as greater use of more idealized bonding angles could lower the rhombicity arbitrarily. We also note that $V(acac)_3$, which is a homoleptic complex, exhibited $|E/D| = 0.26$ [16], nearly as rhombic as heteroleptic $[V(trdta)]^-$.

The HFEPR studies of the trdta complex in frozen aqueous solution can in principle be analyzed in the same fashion. In practice, however, this is not possible because we are uncertain as to the solution state structure. There are multiple ways by which heterogeneity in solution structure of the trdta complex can be obtained. One possibility is the loss of a coordinated carboxylato ligand in aqueous solution [29]. The multiple species that could result from replacement of only one carboxylato ligand by one aqua ligand are shown in cartoon form in Fig. S10. Replacement of a carboxylato

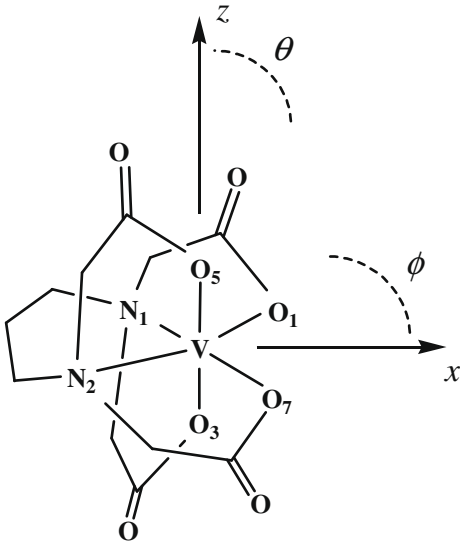

Fig. 5. Molecular coordinate system defined for $[V(trdta)]^-$. The molecular z-axis for $[V(trdta)]^-$ is defined along the O3-V-O5 vector, so that the angle to each ligand from this axis gives θ (note that the actual O3-V-O5 bond angle is 167°, so average angular values from a given atom to V-O3 and V-O5 are used for θ). The plane normal to the O3-V-O5 vector is defined as the molecular xy plane, with the molecular x-axis defined as half of the N1-V-N2 bond angle to give ϕ.

Table 2
Ligand-field parameters (in cm^{-1}) using the AOM for aminocarboxylate complexes of V(III).

Ligand-field parameters	$[V(trdta)]^-$	$[V(edta)(H_2O)]^-$
ζ	140	200[d]
B, C		
Method A[a]	–	340, 1700
Method B[b]	580, 2900	580, 2320
Method C[c]	–	595, 2380
e_σ*(aqua O)*		
Method A[a]		7000
Method B[b]	NA	7000
Method C[c]		6000
$e_{\pi s}$, $e_{\pi c}$*(carboxy O)*		
Method A[a]		1200, 0
Method B[b]	NA	0, 1200
Method C[c]		0, 910
e_σ*(carboxy O)*		
Method A[a]	–	7700
Method B[b]	9100	7700
Method C[c]	–	7180
e_{ns}, e_{nc}*(carboxy O)*		
Method A[a]	–	1700, 1000
Method B[b]	2100, 1300	1000, 1700
Method C[c]	–	660, 1100
e_σ*(amine N)*		
All Methods	6700	5800
Calculated D, E		
Method A[a]	–	+1.85, 0.25
Method B[b]	+5.63, 1.78	+1.48, 0.34
Method C[c]	–	+1.36, 0.33

[a] For only the edta complex, Method A uses the complete set of parameters provided by Schönherr and co-workers [38] along with their geometric model for $[V(edta)(H_2O)]^-$, provided by Prof. Schönherr. For the aqua O donor, anisotropic π-bonding is approximated by $e_{\pi c} = 0$. For the carboxy O donors, anisotropic π-bonding is approximated by $e_{\pi c} \approx 0.6 e_{\pi c}$. The value for *C* is fixed at 5.0*B* [38].

[b] For the trdta complex, only Method B is relevant, and it uses the bonding parameters provided by Schönherr and co-workers [38] without modification and the geometrical model shown in Fig. 5 and described in the text and in Table S1. The value for *C* is thus fixed at 5.0*B* [38]; use of the same parameters with $C = 2730\ cm^{-1}$ ($C = 4.7B$ [34]) gives the same zfs: $D = +5.65\ cm^{-1}$, $E = +1.77\ cm^{-1}$.For the edta complex, Method B uses the bonding parameters provided by Schönherr and co-workers [38] without modification, except for a change of orientation. The direction of the aqua ligand is here along *z*, rather than *x*, so that the values of $e_{\pi s}$ and $e_{\pi c}$ are reversed for the O donor ligands. The geometrical model is shown in Fig. 6 and described in the text and in Table S1. Detailed angular parameters are given in Table S1. Additionally, the value for *B* is derived by fitting the electronic transitions observed here. The value for *C* is fixed at 4.7*B* [34].

[c] For only the edta complex, Method C uses bonding parameters derived from fitting the electronic transitions with the values provided by Schönherr and co-workers [24,38] as only a starting point. The geometrical model used is as in Method B.

[d] For the edta complex, use of $\zeta = 140\ cm^{-1}$, the value appropriate for the $trdta^{4-}$ complex, gives for Method A (with $C = 5.0B$ [38]): $D = +0.91\ cm^{-1}$, $E = +0.12\ cm^{-1}$; for Method B (with $C = 2730\ cm^{-1} = 4.7B$ [34]): $D = +0.70\ cm^{-1}$, $E = +0.17\ cm^{-1}$; for Method C (with $C = 2800\ cm^{-1} = 4.7B$ [34]): $D = +0.65\ cm^{-1}$, $E = +0.16\ cm^{-1}$. Thus an increase in the value of ζ and/or a decrease in the value of *C*, possible for Methods B and C, is needed to achieve the experimental zfs. The choice of $C = 4.0B$ and $\zeta = 200\ cm^{-1}$, nearly the free-ion value, leads to zfs that is close to experiment.

ligand by an aqua ligand was explored by changing the corresponding AOM bonding parameters, which showed that the values for *D* and/or *E* could change significantly. Another possibility is more subtle and cannot be as easily treated by the AOM, namely changes in the conformation of the 1,3-diaminopropane chelate ring. This structural phenomenon has been shown for Fe(III) complexes of trdta [48,49]. These conformers are described in the caption to Fig. S10 and could lead to spectroscopically similar, but distinct species observable by HFEPR in frozen solution.

The HFEPR results for microcrystalline $Na[V(edta)(H_2O)] \cdot 3H_2O$ did not show any heterogeneity and we thus associate the results with the crystallographically characterized species (see Section 2).

In the case of this seven-coordinate edta complex, a geometrical model was chosen in which the molecular *z*-axis is defined along the V-O(aqua) vector, given that the aqua ligand is unique, and the molecular *x*-axis is defined along the V-O1 vector (see Fig. 6; the specific angular parameters are given in Table S1). As mentioned above, we have also employed the model of Schönherr and co-workers [24,38], in which the molecular *x*-axis is along the V-O(aqua) vector.

Three methods were employed to fit the electronic absorption data and extract zfs parameters for $[V(edta)(H_2O)]^-$. In the first case, Method A, the geometrical model of Schönherr and co-workers [24,38] and their refined parameter set [38] was used without modification. This method was possible only for $[V(edta)(H_2O)]^-$, as we did not have the exact geometrical model for $[V(trdta)]^-$. In Method B, our own geometrical models were used (see above and Figs. 5 and 6), along with the AOM bonding parameters of Schönherr and co-workers [38] (modified only to account for the change in coordinate system), but the Racah *B* parameter was allowed to vary freely. This model was employed because the value for *B* reported was rather low, 340 cm^{-1}, which is less than 40% of the free-ion value [34,36]. In the third case, Model C, the AOM bonding parameters for the carboxylato ligands were also allowed to vary, although the amino ligands were fixed at the reported values.

As seen in Table S2, all of these models effectively fit the observed electronic absorption spectra. Use of Method B led to a fit value for $B = 580\ cm^{-1}$, which is the same as that for $[V(trdta)]^-$, and is thus more reasonable. Use of Method C led to different bonding parameters, but none that was drastically different from those reported and with $B = 595\ cm^{-1}$. The fit parameters are summarized in Table 2, which also gives the zfs calculated by inclusion of spin-orbit coupling. The logical choice for this parameter is $\zeta = 140\ cm^{-1}$, as it is the same as employed in $[V(trdta)]^-$, but this

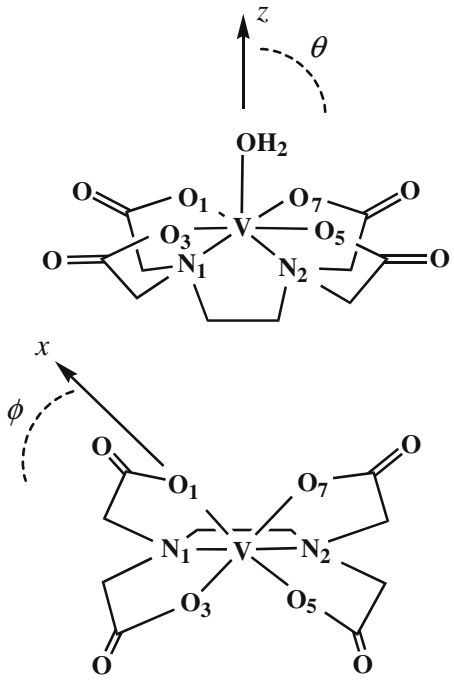

Fig. 6. Molecular coordinate system defined for $[V(edta)(H_2O)]^-$. The molecular *z*-axis for $[V(edta)(H_2O)]^-$ is defined along the V-OH_2 vector, so that the angle to each ligand from this axis gives θ (see upper drawing). The projection of the O1,3,5,7 and N1,2 ligands onto a plane normal to the V-OH_2 vector is defined as the molecular *xy* plane, with the molecular *x*-axis defined along the V-O1 vector, so that an angle in this plane gives ϕ (see lower drawing, in which the axial H_2O ligand in the foreground is omitted for clarity).

led to zfs that was significantly lower than experimentally observed, regardless of the method used (see Table 2). In order to obtain the observed zfs, it was necessary to increase the value of ζ to 200 cm^{-1}, nearly the free-ion value [35], and, for Methods B and C, also to reduce the value of C, to $C = 4.0B$, which is not an unreasonable ratio. With these modifications, the match between the observed and calculated zfs magnitude is quite good (see Table 2). Method A, due to its smaller B value, perhaps unreasonably so, and consequent lower-lying excited states from ^3P, gives the largest zfs, which is the closest to the larger, solution value, while Methods B and C give better fits to the smaller, solid state value. Also important is that the calculated sign of D is positive, which matches experiment for the solution (it could not be determined for the solid, but D is likely positive as well). We also note that these methods do tend to overestimate the rhombicity of the zfs, with $|E/D| > 0.2$ for Methods B and C, while the solid gave $|E/D| = 0.1$ and the solution was axial. It is possible that asymmetry in bonding and geometry that is locked into the crystal structure averages out in solution. Use of the AOM, or other computational methods, such as DFT, in combination with geometry optimized structures could be used to test this possibility, however, that type of computational investigation is beyond the scope of this work. In any case, as with the trdta complex, the exact solution structure is unknown. Geometries such as capped trigonal prism or 4:3 piano stool [42] can exhibit a variety of twist angles, as described by Shimoi et al. [26,41], and these could affect the spin Hamiltonian parameters subtly. We have explored a more dramatic change, namely the possibility that $[V(edta)(H_2O)]^-$ exhibits pentagonal bipyramidal geometry (pbp) in solution. We used as a rough structural model the Fe(III) analog, which does adopt this geometry. Among the several such structures reported, we chose that of $Li[Fe(edta)(H_2O)] \cdot 3H_2O$[50]. Use of the AOM parameters derived above for the actual structure of the V(III) complex does yield NIR bands at 7500–8000 cm^{-1} and at 9650 cm^{-1}, and several visible bands in the 23,000–28,000 cm^{-1} range, although the band at 12,500 cm^{-1} is calculated too low by ~1800 cm^{-1}. Furthermore, use of similar SOC to the above affords zfs that is much larger than that observed (~6 cm^{-1} for $\zeta = 200$ cm^{-1}). We conclude that pbp geometry is unlikely for $[V(edta)(H_2O)]^-$, although distortion towards pbp geometry might lead to the higher zfs observed in solution. In contrast to $[V(trdta)]^-$, for which spin Hamiltonian parameters are known for a few analogous complexes [16,19], to our knowledge, no comparison data are available for seven-coordinate V(III). Lastly, we note that our ligand-field model does not include spin–spin coupling [51], among other simplifications, which might increase the zfs for a given value of spin-orbit coupling.

4. Conclusions

The V(III) ion is paramagnetic, but not readily suited to conventional EPR, due to its integer-spin ground state ($S = 1$) with large zfs. High-frequency and -field EPR (HFEPR), however, has the ability to study such systems effectively. We have applied HFEPR to investigate three aminocarboxylate complexes of V(III): $Na[V(trdta)] \cdot 3H_2O$, $Na[V(edta)(H_2O)] \cdot 3H_2O$, and $[V(nta)(H_2O)_3] \cdot 4H_2O$. While $[V(nta)(H_2O)_3] \cdot 4H_2O$ did not yield interpretable spectra in the solid state due to spin exchange, both the trdta and edta complexes gave readily interpretable spectra in this form. All three complexes produced frozen aqueous solution spectra at concentrations of ~200 mM. These HFEPR spectra are the first, to our knowledge, of V(III) in solution, demonstrating the potential for applying HFEPR to the study of V(III) complexes in aqueous solution.

For the edta and trdta complexes, the availability of both solid state and frozen solution HFEPR spectra allowed precise determination of spin Hamiltonian parameters. These parameters, in combination with very insightful previous studies by Schönherr and coworkers [24,38], who analyzed the electronic absorption spectra of these complexes, and provided ligand-field parameters for them, has made it possible to provide a complete picture of the electronic structure of V(III) in both $Na[V(trdta)] \cdot 3H_2O$ and $Na[V(edta)(H_2O)] \cdot 3H_2O$, i.e., the solid state forms that have been structurally characterized. Qualitatively, and thus applicable to both solid state and frozen solution species, six-coordinate V(III) complexes with O,N donor atoms show no electronic absorption band in the NIR region, and exhibit relatively large magnitude zfs of ($D \geqslant 5$ cm^{-1}), while analogous seven-coordinate complexes do have a NIR absorption band and show relatively smaller magnitude zfs ($D < 2$ cm^{-1}).

This correlation of electronic structure with coordination environment for aminocarboxylate complexes of V(III) is important since these complexes are of interest as models for biologically and medicinally relevant forms of this ion. It should thus be possible to employ optical spectroscopic methods (electronic absorption, MCD) and magnetic resonance (HFEPR) to interrogate V(III) sites in intact biological systems as we and others have demonstrated for model complexes.

5. Abbreviations

Chemical terms

acac	2,4-pentanedionate
edta	ethylenediamine-*N*,*N*,*N*′,*N*′-tetraacetate (1,2-diaminoethane-*N*,*N*,*N*′,*N*′-tetraacetate)
nta	nitrilotriacetate (α,α′,α″-trimethylaminetricarboxylate)
trdta	trimethylenediamine-*N*,*N*,*N*′,*N*′-tetraacetate
THF	tetrahydrofuran

Other terms

AOM	angular overlap model
EMR	electron magnetic resonance
DDN	double precision d^n electronic configuration program
HFEPR	high-frequency and -field electron paramagnetic resonance
MCD	magnetic circular dichroism
NHMFL	National High Magnetic Field Laboratory
SOC	spin-orbit coupling
Zfs	zero-field splitting

Acknowledgments

H.-F.H., C.-C.W., and K.-Y.C. gratefully acknowledge the National Science Council in Taiwan for funding this work (NSC 96-2113-M-006-011). HFEPR studies were supported by the National High Magnetic Field Laboratory, which is funded by the NSF through Cooperative Agreement DMR 0654118, the State of Florida, and the DOE. The 25-T resistive magnet was funded by the W.M. Keck Foundation. J.T. and J.K. acknowledge NHMFL IHRP grant 5062. We thank Prof. Dr. Thomas Schönherr, Heinrich-Heine-University of Düsseldorf, Germany, for providing a reference and for many helpful discussions.

Appendix A. Supplementary material

Supplementary data associated with this article can be found, in the online version, at doi:10.1016/j.jinorgbio.2009.01.016.

References

[1] T. Hirao, Coord. Chem. Rev. 237 (2003) 1.
[2] N.D. Chasteen, Struct. Bond. 53 (1983) 105–138.
[3] D.C. Crans, J.J. Smee, E. Gaidamauskas, L. Yang, Chem. Rev. 104 (2004) 849–902.
[4] H. Michibata, N. Yamaguchi, T. Uyama, T. Ueki, Coord. Chem. Rev. 237 (2003) 41–51.

[5] P. Frank, E.J. Carlson, R.M.K. Carlson, B. Hedman, K.O. Hodgson, J. Inorg. Biochem. 102 (2008) 809–823.
[6] S.W. Taylor, C.J. Hawkins, D.L. Parry, J.H. Swinehart, G.R. Hanson, J. Inorg. Biochem. 56 (1994) 97–116.
[7] M. Henez, Hoppe-Seylers Z. Physiol. Chem. 72 (1911) 494–501.
[8] V. Monga, K.H. Thompson, V.G. Yuen, V. Sharma, B.O. Patrick, J.H. McNeill, C. Orvig, Inorg. Chem. 44 (2005) 2678–2688.
[9] P. Buglyó, D.C. Crans, E.M. Nagy, R.L. Lindo, L. Yang, J.J. Smee, W. Jin, L.-H. Chi, M.E.G. Godzala III, G.R. Willsky, Inorg. Chem. 44 (2005) 5416–5427.
[10] K.H. Thompson, J.H. McNeill, C. Orvig, Chem. Rev. 99 (1999) 2561–2571.
[11] T. Storr, D. Mitchell, P. Buglyó, K.H. Thompson, V.G. Yuen, J.H. McNeill, C. Orvig, Bioconjugate Chem. 14 (2003) 212–221.
[12] N.D. Chasteen, in: L.J. Berliner, J. Reuben (Eds.), Biological Magnetic Resonance, vol. 3, Plenum, New York, 1981, pp. 53–119.
[13] H. Ohta, M. Yoshida, S. Okubo, T. Ito, H. Takagi, Y. Ajiro, J. Phys. Conf. Ser. 51 (2006) 15–22.
[14] J. Krzystek, S.A. Zvyagin, A. Ozarowski, S. Trofimenko, J. Telser, J. Magn. Reson. 178 (2006) 174–183.
[15] J. Krzystek, A. Ozarowski, J. Telser, Coord. Chem. Rev. 250 (2006) 2308–2324.
[16] J. Krzystek, A.T. Fiedler, J.J. Sokol, A. Ozarowski, S.A. Zvyagin, T.C. Brunold, J.R. Long, L.-C. Brunel, J. Telser, Inorg. Chem. 43 (2004) 5645–5658.
[17] P.L.W. Tregenna-Piggott, H. Weihe, J. Bendix, A.-L. Barra, H.-U. Güdel, Inorg. Chem. 38 (1999) 5928–5929.
[18] P.L.W. Tregenna-Piggott, S.P. Best, H.-U. Güdel, H. Weihe, C.C. Wilson, J. Solid State Chem. 145 (1999) 460–470.
[19] P.L.W. Tregenna-Piggott, D. Spichiger, G. Carver, B. Frey, R. Meier, H. Weihe, J.A. Cowan, G.J. McIntyre, G. Zahn, A.-L. Barra, Inorg. Chem. 43 (2004) 8049–8060.
[20] P.L.W. Tregenna-Piggott, G. Carver, Inorg. Chem. 43 (2004) 8061–8071.
[21] R. Beaulac, P.L.W. Tregenna-Piggott, A.L. Barra, H. Weihe, D. Luneau, C. Reber, Inorg. Chem. 45 (2006) 3399–3407.
[22] J. Telser, L.A. Pardi, J. Krzystek, L.-C. Brunel, Inorg. Chem. 37 (1998) 5769–5775.
[23] J. Krzystek, J. Telser, J. Magn. Reson. 162 (2003) 454–465.
[24] R. Meier, M. Boddin, S. Mitzenheim, V. Schmid, T. Schönherr, J. Inorg. Biochem. 69 (1998) 249–252.
[25] J.C. Robles, Y. Matsuzaka, S. Inomata, M. Shimoi, W. Mori, H. Ogino, Inorg. Chem. 32 (1993) 13–17.
[26] M. Shimoi, Y. Saito, H. Ogino, Bull. Chem. Soc. Jpn. 64 (1991) 2629–2634.
[27] K. Okamoto, J. Hidaka, M. Fukagawa, K. Kanamori, Acta Crystallogr. C48 (1992) 1025–1027.
[28] G. Schwarzenbach, J. Sandera, Helv. Chim. Acta 36 (1953) 1089–1101.
[29] K. Kanamori, K. Ino, H. Maeda, K. Miyazaki, M. Fukagawa, J. Kumada, T. Eguchi, K.-i. Okamoto, Inorg. Chem. 33 (1994) 5547–5554.
[30] S.A. Zvyagin, J. Krzystek, P.H.M. van Loosdrecht, G. Dhalenne, A. Revcolevschi, Physica B 346–347 (2004) 1–5.
[31] J. Krzystek, J. Telser, L.A. Pardi, D.P. Goldberg, B.M. Hoffman, L.-C. Brunel, Inorg. Chem. 38 (1999) 6121–6129.
[32] A. Abragam, B. Bleaney, Electron Paramagnetic Resonance of Transition Ions, Dover Publications, Inc., New York, 1986.
[33] J. Baranowski, T. Cukierda, B. Jezowska-Trzebiatowska, H. Kozlowski, Chem. Phys. Lett. 39 (1976) 606–608.
[34] B.N. Figgis, M.A. Hitchman, Ligand Field Theory and Its Applications, Wiley VCH, New York, 2000.
[35] J. Bendix, M. Brorson, C.E. Schäffer, Inorg. Chem. 32 (1993) 2838–2849.
[36] F.E. Mabbs, D. Collison, Electron Paramagnetic Resonance of d Transition Metal Compounds, Elsevier, Amsterdam, 1992.
[37] C.E. Schäffer, Struct. Bond. 5 (1968) 68–95.
[38] T. Schönherr, V. Schmid, R. Meier, Spectrochim. Acta Part A 54 (1998) 1659–1669.
[39] K. Miyoshi, J. Wang, T. Mizuta, Inorg. Chim. Acta 228 (1995) 165–172.
[40] R.E. Shepherd, W.E. Hatfield, D. Ghosh, C.D. Stout, F.J. Kristine, J.R. Ruble, J. Am. Chem. Soc. 103 (1981) 5511–5517.
[41] M. Shimoi, S. Miyamoto, H. Ogino, Bull. Chem. Soc. Jpn. 64 (1991) 2549–2550.
[42] E.B. Dreyer, C.T. Lam, S.J. Lippard, Inorg. Chem. 18 (1979) 1904–1908.
[43] H.-F. Hsu, W.-C. Chu, C.-H. Hung, J.-H. Liao, Inorg. Chem. 42 (2003) 7369–7371.
[44] U. Rychlewska, B. Warżajtis, D. Cvetić, D.D. Radanović, D.M. Gurešić, M.I. Djuran, Polyhedron 26 (2007) 1717–1724.
[45] K. Park, M.A. Novotny, N.S. Dalal, S. Hill, P.A. Rikvold, Phys. Rev. B 65 (2001) 014426.
[46] J. Krzystek, J.-H. Park, M.W. Meisel, M.A. Hitchman, H. Stratemeier, L.-C. Brunel, J. Telser, Inorg. Chem. 41 (2002) 4478–4487.
[47] P.J. Desrochers, J. Telser, S.A. Zvyagin, A. Ozarowski, J. Krzystek, D.A. Vicic, Inorg. Chem. 45 (2006) 8930–8941.
[48] K. Kanamori, N. Ukita, K. Kawai, S. Taguchi, K. Goto, T. Eguchi, M. Kishita, Inorg. Chim. Acta 186 (1991) 205–208.
[49] R. Meier, J. Maigut, B. Kallies, N. Lehnert, F. Paulat, F.W. Heinemann, G. Zahn, M.P. Feth, H. Krautscheid, R.v. Eldik, Chem. Commun. (2007) 3960–3962.
[50] M.D. Lind, M.J. Hamor, T.A. Hamor, J.L. Hoard, Inorg. Chem. 3 (1964) 34–43.
[51] D. Ganyushin, F. Neese, J. Chem. Phys. 125 (2006) 024103.